

Controlling the chimera form in the Leaky Integrate-and-Fire model

A. Provata · Ch. G. Antonopoulos ·
P. Vlamos

Received: date / Accepted: date

Abstract We study the influence of broken connectivity and frequency disorder in systems of coupled neuronal oscillators. Under nonlocal coupling, systems of nonlinear oscillators, such as Kuramoto, FitzHugh-Nagumo or Integrate-and-Fire oscillators, demonstrate nontrivial synchronization patterns. One of these patterns is the “chimera state”, which consists of coexisting coherent and incoherent domains. In networks of biological neurons, the connectivity is not always perfect, but might be locally broken, or interrupted due to pathologies, neuron degenerative disorders or accidents. Our simulations show that destructed connectivity drastically affects synchronization, driving the coherent parts of the chimera state to cover symmetrically the region where the anomaly is located. The network synchronization decreases with the size of the destructed region as evidenced by the Kuramoto synchronization index. To the contrary, when keeping the connectivity of all nodes intact, altering the frequency in a block of oscillators drives the incoherent part of the chimera state toward the anomaly. This work is in-line with recent dynamical approaches aiming to locate anomalies in the structure of brain networks, in particular when the anomalies have small, difficult-to-detect sizes.

Keywords : Leaky Integrate-and-Fire Model · Synchronization · Chimera States · Control · Kuramoto Synchronization Index

A. Provata
Institute of Nanoscience and Nanotechnology, National Center for Scientific Research “Demokritos”, GR-15341, Athens, Greece
E-mail: a.provata@inn.demokritos.gr

Ch. G. Antonopoulos
Department of Mathematical Sciences, University of Essex, Wivenhoe Park, CO4 3SQ, United Kingdom
E-mail: canton@essex.ac.uk

P. Vlamos
Department of Informatics, Ionian University, Plateia Tsirigoti 7, GR-49100, Corfu, Greece
E-mail: vlamos@ionio.gr

1 Introduction

Intensive numerical studies of synchronization patterns in networks of interacting neurons have led to the recent discovery of the so called “chimera states”. These are states where domains of coherent oscillators alternate with incoherent ones and this phenomenon is observed even in the case where all oscillators are identical and identically linked. Chimera states were first observed in 2002 by Kuramoto when he was studying synchronization properties in networks of neuronal oscillators [1]. In this work Kuramoto and Battogtokh used the phase oscillator to assimilate the behavior of neurons. Later on, chimera states were found in other neuronal models, such as in the FitzHugh-Nagumo [2–4], Hindmarsh-Rose [5,6], Van der Pol [7] and in the Leaky Integrate-and-Fire (LIF) models [8–11].

While in the original studies the network had the simple form of a 1D chain closed in a ring arrangement, later works used more complex connectivities in an effort to approach the realistic connectivities of brain neurons. More complex connectivities include 2D square lattices [12], 3D cubic lattices [13–15], fractal geometries [16–18] and other complex structures [6,19–21]. Recent advances on the emergence and structure of chimera states in neuronal dynamics are reported in review articles [22–24].

The complexity in the connectivity was mainly motivated by experimental evidence on brain structure from Magnetic Resonance Imaging (MRI) [25–27] and Electroencephalography (EEG) studies [28–30]. So far, the presence of chimera states has been linked with the onset of epileptic seizures [31–33], while they have been associated with the unihemispheric sleep of birds and mammals [34,35].

Due to prospective applications in systems of brain neurons, the control of chimeras (their existence and patterns) has gained a lot of attention in recent years [18,36,37]. In particular, in ref. [37] the authors study the control of phase oscillators, by introducing a modification in the links of one oscillator, making it unidirectional. In the case of phase oscillators, they show that the modified oscillator acts as a pacemaker that attracts the incoherent parts of the chimera. In ref. [36], the authors introduce a block of excitable elements in a ring of FitzHugh-Nagumo limit-cycle oscillators linked nonlocally in a ring. They also report that the incoherent part of the chimera state is attracted by the block of excitable units. Motivated by these findings, we study here the control of a LIF-oscillator network. Our numerical results show that local modifications in the connectivity lead to shifting the chimera pattern, in a way that the modified region attracts the coherent part of the chimera state. To the contrary, when the dynamics in a block of nodes is locally modified, then the modified block attracts the incoherent part of the chimera states.

In the next section, the Leaky Integrate-and-Fire model is introduced and the nonlocal coupling scheme in 1D is presented. The parameter values for single and multichimera states are determined and the Kuramoto synchronization index is introduced and discussed. In Sec. 3, the modifications to the nonlocal coupling scheme are introduced and the results of the simulations are

presented in two subsections: a) in Sec. 3.1, where the parameters favor the formation of a single chimera state and b) in Sec. 3.2, where the parameters favor a multichimera state. The numerical simulations indicate that in both cases the center of a coherent region is driven toward the disordered block. In Sec. 4, a block of LIF nodes with modified frequency is introduced. In the case of a single chimera state, we show that the center of the incoherent region is driven toward the block. In the Conclusions section, our main findings are highlighted and open problems are discussed.

2 The model

To model the exchange of electrical and chemical signals between neurons, we use the Leaky Integrate-and-Fire model. This is a simple scheme which describes the primary oscillations of the membrane potential during the integration and discharging phases in the activity of a neuron. The basic mechanism and corresponding equations were introduced by Louis Lapicque in 1907 [38, 39]. The potential cycles include the integration phase, which is characterized by an exponential increase of the potential, followed by the abrupt resetting phase to the resting state [8,9]. According to the LIF model, one linear ODE, Eq. 1a, and one resetting condition, Eq. 1b are used to describe the evolution of the membrane potential $u(t)$ of a single neuron [16]:

$$\frac{du(t)}{dt} = \mu - u(t), \quad (1a)$$

$$\lim_{\epsilon \rightarrow 0^+} u(t + \epsilon) \rightarrow u_0, \quad \text{when } u(t) \geq u_{\text{th}}. \quad (1b)$$

In Eq. 1a, the constant μ denotes the fixed point where the potential tends when $t \rightarrow \infty$ if the resetting condition is not applied. In Eq. 1b, u_{th} denotes the threshold potential: the $u(t)$ values are reset to the resting potential u_{rest} if they exceed u_{th} . The resetting to the resting state is instantaneous and the period T_s of the single neuron is calculated from Eqs. 1 as [16]:

$$T_s = \ln [(\mu - u_{\text{rest}})/(\mu - u_{\text{th}})]. \quad (2)$$

2.1 Coupling Scheme of LIF Network

When many oscillators, $i = 1, \dots, N$, are coupled in a network, a connectivity matrix σ_{ij} is employed to define the strength of the coupling between neurons i and j . If we denote by $u_i(t)$ the potential of neuron i at time t and by $u_{\text{th}}(i)$ the individual threshold of each neuron i , then the equations which describe the network co-evolution are:

$$\frac{du_i(t)}{dt} = \mu - u_i(t) - \frac{1}{N_i} \sum_{j=1}^N \sigma_{ji} [u_j(t) - u_i(t)], \quad (3a)$$

$$\lim_{\epsilon \rightarrow 0^+} u_i(t + \epsilon) \rightarrow u_{\text{rest}}, \quad \text{when } u_i(t) \geq u_{\text{th}}(i). \quad (3b)$$

In Eq. 3a, each neuron is connected with all other neurons, $j = 1, \dots, N$ in the system, while $N_i = \sum_{j=1}^N \sigma_{ji}$ is the normalization factor applied to all connections.

In earlier studies, the individual LIF oscillators were coupled in a ring chain containing N neuronal oscillators with identical nonlocal coupling among them and with identical threshold values [10,16]. In this study, we first introduce connectivity disorder in a block of B elements located in the interval $I_B = [N/2 - B/2, N/2 + B/2]$. The disorder amounts to breaking locally some of the connections with probability p . In this case, the connectivity matrix takes the form:

$$\sigma_{ij} = \begin{cases} \sigma, & \text{for } i - R < j < i + R, \\ 0, & \text{for } j \in I_B \text{ and } \forall i \text{ with probability } p, \\ \sigma, & \text{for } j \in I_B \text{ and } \forall i \text{ with probability } (1 - p), \\ 0, & \text{elsewhere.} \end{cases} \quad (4)$$

More specifically, Eq. 4 denotes that each element is connected with R neighbors to its left and R neighbors to its right, except the elements that belong to the interval I_B . This interval is of size B and is located around the central node of the ring at positions $[N/2 - B/2, \dots, N/2 + B/2]$. The nodes i residing in this interval communicate nonlocally with the other nodes in the network, $\sigma_{ij} = \sigma$ for $i - R < j < i + R$, without receiving information from other nodes, i.e., $\sigma_{ij} = 0$ when $j \in I_B$. This disruption in the connectivity takes place with some probability p , common to all elements in the interval I_B . The results on broken connectivity are discussed in Sec. 3.

2.2 Modification in the threshold potentials

A second modification in the model refers to a local disorder in the frequencies of the neurons residing in an interval I_{th} of size H , located at position $I_{\text{th}} = [N/2 - H/2, N/2 + H/2]$. As the frequency is intrinsically linked to the threshold potential via Eq. 2, it is easy to modify the frequency by modifying locally the threshold values as follows:

$$u_{\text{th}}(i) = \begin{cases} v_1, & \text{when } i \in I_{\text{th}}, \\ v_2, & \text{elsewhere.} \end{cases} \quad (5)$$

More specifically, Eq. 5 indicates that all the elements in positions $[N/2 - H/2, \dots, N/2 + H/2]$ have threshold v_1 , while the rest have threshold v_2 . The perturbed interval contains H elements and is located around the central element of the ring which is at position $N/2$. The results of this perturbation in the dynamics are discussed in Sec. 4.

2.3 The Kuramoto Synchronization Index

One of the first indices to quantify the presence of chimera states is the Kuramoto synchronization index $Z(t)$, also known as Kuramoto order parameter [1,22]. To use the Kuramoto index one needs to define the phase $\phi(t)$ during the oscillation period. In the LIF model, the phase $\phi_i(t)$ of oscillator i is defined in terms of the time dependent potential $u_i(t)$ as [17]:

$$\phi_i(t) = \frac{2\pi u_i(t)}{u_{\text{th}}(i)}. \quad (6)$$

The global Kuramoto synchronization index is then defined as:

$$Z(t) = \frac{1}{N} \left| \sum_{i=1}^N e^{i\phi_i(t)} \right|, \quad (7)$$

where $|\cdot|$ stands for the magnitude of the complex number in the argument. $Z(t)$ denotes the time dependent degree of synchronization in the network. Namely, if $Z = 1$, the dynamics in the network is synchronized, if $Z = 0$ the dynamics is asynchronous and if $0 < Z < 1$, the dynamics is partially synchronous and a chimera state is formed. Often, an average synchronization index, $\langle Z \rangle$, is defined on a time interval ΔT for statistical reasons:

$$\langle Z \rangle = \frac{\sum_{\Delta T} Z(t)}{\Delta T}. \quad (8)$$

One weakness of the average Kuramoto index is the false estimation of synchronization when traveling patterns are formed in the network, which is often the case when chimera states are present. Another drawback is that the Kuramoto index defines full synchronization when all nodes have exactly the same phase and does not distinguish the frequency synchronization, where all elements have the same frequency but keep a constant phase difference in time.

Other than the Kuramoto index, the mean phase velocity profile is a dependable indicator of coherence. For an oscillator i who has performed C_i complete oscillations in time ΔT , the mean phase velocity ω_i is defined as:

$$\omega_i = \frac{2\pi C_i(\Delta T)}{\Delta T}. \quad (9)$$

Since the mean phase velocity ω_i and frequency f_i of an oscillator are proportional with a constant factor of 2π , namely:

$$\omega_i = 2\pi f_i, \quad (10)$$

the terms ‘‘mean phase velocity’’ and ‘‘frequency’’ are hereafter used interchangeably.

The difference between the maximum and minimum mean phase velocity in the system, $\Delta\omega = \omega_{\text{max}} - \omega_{\text{min}}$ is also a reliable indicator and establishes the existence of a chimera state if $\Delta\omega > 0$ (and similarly for the frequency

difference). Other measures of synchronization include the ratios N_{coh} (N_{incoh}) of coherent (incoherent) elements, the integrated coherence measure and the Laplacian measure [40–42].

In the present study, we only discuss patterns which are stable in time and the elements in the coherent region are phase as well as frequency synchronous. Therefore, the Kuramoto index is particularly suitable for quantifying the chimera states.

The working parameters used in this study are: $\mu = 1$, $u_{\text{rest}} = 0$, $N = 500$ and $R = 170$. The rest of the parameters, namely, $u_{\text{th}}(i)$, σ , p , B and H , will be varied in the next two sections.

3 Chimera states under broken connectivity

As discussed in Sec. 2, locally broken connectivity in the network can be realized with the use of a specific connectivity matrix. The connectivity matrix we use here as an exemplary case is given by Eq. 4. The region of broken links has length B which ranges from $B = 0$ (unbroken, nonlocal case) to $B = 20$. All other parameter are as defined in the working parameter set in Sec. 2. In the next two subsections, we set the parameter σ to values which produce single chimeras in Sec. 3.1 and double chimeras in Sec. 3.2.

3.1 Single chimeras

For the emergence of single chimeras, the coupling strength is set to $\sigma = 0.7$ and the threshold potential is fixed to $u_{\text{th}} = 0.98$, common for all nodes. For these parameters, when the connectivity is nonlocal (without modifications), a single chimera state is observed [10], shown in Fig. 1a.

Figure 1 presents a comparison of the dynamics between unbroken connectivities and locally broken in rows a) for $B = 0$ and b) for $B = 10$, respectively. All other parameters in rows a) and b) are identical and the oscillators start from the same initial conditions. In row a), a chimera state with one coherent and one incoherent domain is formed. In this case, the coherent domain is formed in the right side of the system. When the connectivity is broken at positions $I_B = [245 - 254]$ in row b), the coherent domain moves toward the area where the broken connectivity is located, and the coherent and incoherent domains are positioned symmetrically around this structural anomaly. In row b), the oscillators which belong to the area I_B are colored in red in the profile snapshot (left panel). Note that the points in I_B are scattered, as the oscillators in this domain do not receive input from the rest of the system and, consequently, they follow independent dynamics, based on their own initial conditions. In the spacetime plot of row b), the oscillators which belong to the block I_B are clearly discerned as a yellow perpendicular stripe.

In the previous example, the oscillators have started at time $t = 0$ from the same random initial conditions in both cases. We now consider the case

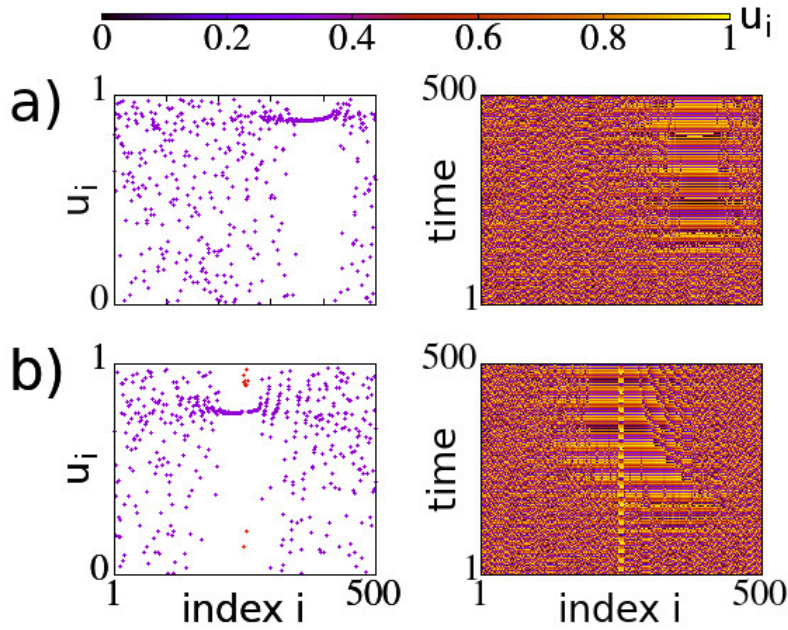


Fig. 1 (Color online) Chimera states in the LIF network with a) nonlocal connectivity, $B = 0$, and b) locally broken connectivity, $B = 10$. Typical profile snapshots (left panels) and spacetime plots (right panels). In b), the broken links are located in the range $[245-254]$. Other parameters are common: $\sigma = 0.7$, $\mu = 1$, u_{rest} , $u_{\text{th}} = 0.98$, $N = 500$ and $R = 170$. In the simulations a) and b) the oscillators start from the same initial conditions, chosen randomly between 0 and u_{th} .

where the system initially runs without the structural anomaly I_B and the connectivity is broken at 500 time units (TUs), after the single chimera has already been established. Moreover, the links in block I_B are broken with a given probability $0 \leq p \leq 1$. Typical results are shown in Fig. 2.

In particular, in all three rows of Fig. 2, the network simulations have run for 500 TUs without broken connectivity. In all cases, a coherent state is established on the right side, as can be seen in the respective spacetime plots. At $t = 500$ TUs the connectivity is broken in the middle of the system (ring), at positions $I_B = [245 - 254]$, with a different breaking probability $p = 1, 0.8$ and 0.5 . The results are as follows:

- In Fig. 2a, the block breaking probability is $p = 1.0$ and all links directed toward the block are broken. In this case, the spacetime plot (right panel) indicates that the coherent part is first formed on the right side of the ring and, when the block connectivity is broken (at $t = 500$ TUs), the coherent part is driven, almost immediately, towards the structural irregularity. At the steady state, the coherent part surrounds the irregularity. The block I_B is evident around the node $i = 250$. The Kuramoto index of synchronization

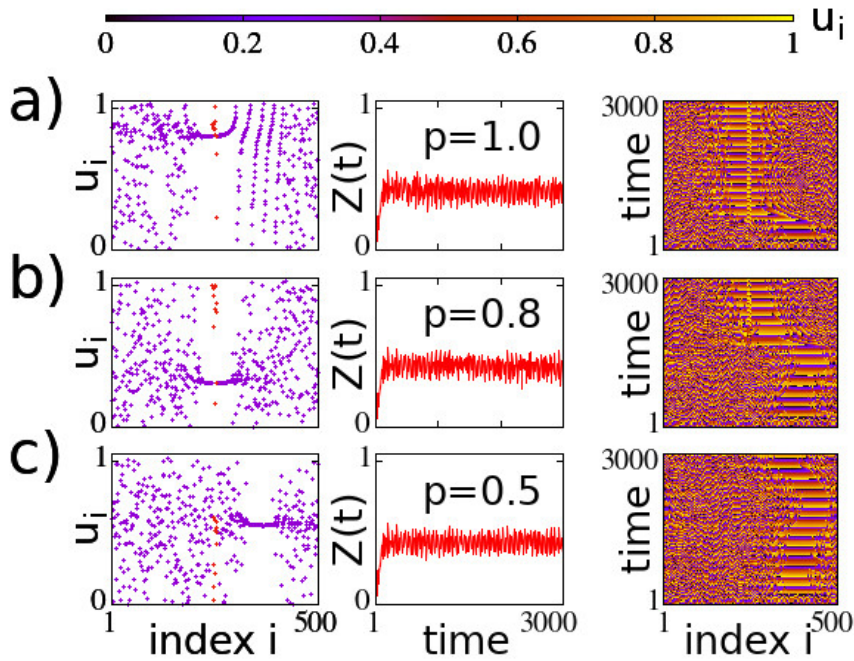


Fig. 2 (Color online) Chimera states in the LIF network with broken connectivity after 500 TUs: a) $p=1.0$, b) $p=0.8$ and c) $p=0.5$. Typical profile snapshots (left panels), Kuramoto index (central panels) and spacetime plots (right panels). The broken links are located in the range [245-254]. All other parameters are as in Fig. 1. All realizations start from the same initial conditions, chosen randomly between 0 and u_{th} .

(central panel) starts from $Z = 0$, when the network elements have random potentials at $t = 0$, and increases as the chimera state is formed. After the chimera formation, the Z -index does not change on average (apart from fluctuations). A typical potential profile can be observed in the left panel, after the establishment of the chimera state; the oscillators which belong to block I_B are clearly discerned in the center of the coherent region and are colored red.

- In Fig. 2b, the links directed towards block I_B were broken with probability $p = 0.8$ after 500 TUs, while for times $0 < t < 500$ the connectivity is kept typically nonlocal, giving rise to the single chimera seen in Fig. 1a. In this case, the coherent region is less strongly attracted by the block, since the structural anomaly is weaker. Here, although the breaking takes place at $t = 500$ TUs, the coherent region stabilizes around the anomaly much later, at about $t = 2000$ TUs; then, the presence of the block becomes evident around element $i \sim 250$, as seen in the spacetime plot. The temporal evolution of the Kuramoto index does not change (see central panel). $Z(t)$ only depends on the relative size of the coherent and incoherent regions

and that is not altered by the introduction of the structural anomaly. The potential profile at the final stage, after the coherent region has surrounded the block I_B , has similar structure as in the case $p = 1$.

- In Fig. 2c, with $p = 0.5$, the breaking probability is even weaker. The block I_B can not attract the coherent region and only causes erratic motion on the position of the (in)coherent regions, as evidenced by the spacetime plot. Note that the position of the block I_B is not visible here, as it is hidden within the incoherent domain. The position of the block I_B is evidenced in the potential profile (left panel), where its elements are colored in red and are indeed found within the incoherent region. The evolution of the Kuramoto index (see central panel) does not change statistically with respect to the previous two cases.

The block size used here, $B = 10$, is just an indicative example. Even, the weakest case, $B = 1$, is enough to cause the drift of the coherent regions toward the block (results not shown).

Thus, we conclude that breaking the incoming connectivity in a block of elements causes the shift of the coherent region toward the block. Therefore, the insertion of a structural deformation of this type can be used to control the position of the coherent/incoherent regions of the chimera. Moreover, the neuronal oscillators that belong to block I_B and do not receive contributions from the rest of the network retain their (uncoupled) frequency and act as pacemakers, dictating to the rest of the network the dynamics of the single oscillator.

3.2 Multichimera states

The parameter choice $\sigma = 0.7$ used in the previous section was important for the emergence of a single chimera state with one coherent and one incoherent region. In this section, we use a higher coupling strength, namely $\sigma = 1.7$, which gives rise to a double chimera state with two coherent and two incoherent regions [10]. Here, we choose to show the effect of increasing the size of block B to 0, 1, 10 and 20. We, then, keep the breaking probability to its highest value, $p = 1$, and all other parameters are as in Sec. 3.1.

For the larger value $\sigma = 1.7$, the nonlocally coupled system supports the multichimera state, as depicted in Fig. 3a. The results for the different B -values are presented in Fig. 3b, c and d. For the chosen initial conditions, the unperturbed system with $B = 0$ presents two coherent/incoherent regions as shown in Fig. 3a. In fact, the spacetime plot demonstrates that, at $t = 0$, one of the incoherent regions is centered around the central node $i = 250$ and, as time increases, the chimera pattern drifts first toward the right and then toward the left.

When a block of broken links is introduced, see rows b), c) and d) in Fig. 3, the 2-chimera pattern drifts until one of the coherent regions is stabilized around the block where the links are broken. In fact, in Fig. 3b, c and d the system for the first 500 TUs has uninterrupted nonlocal connectivity and

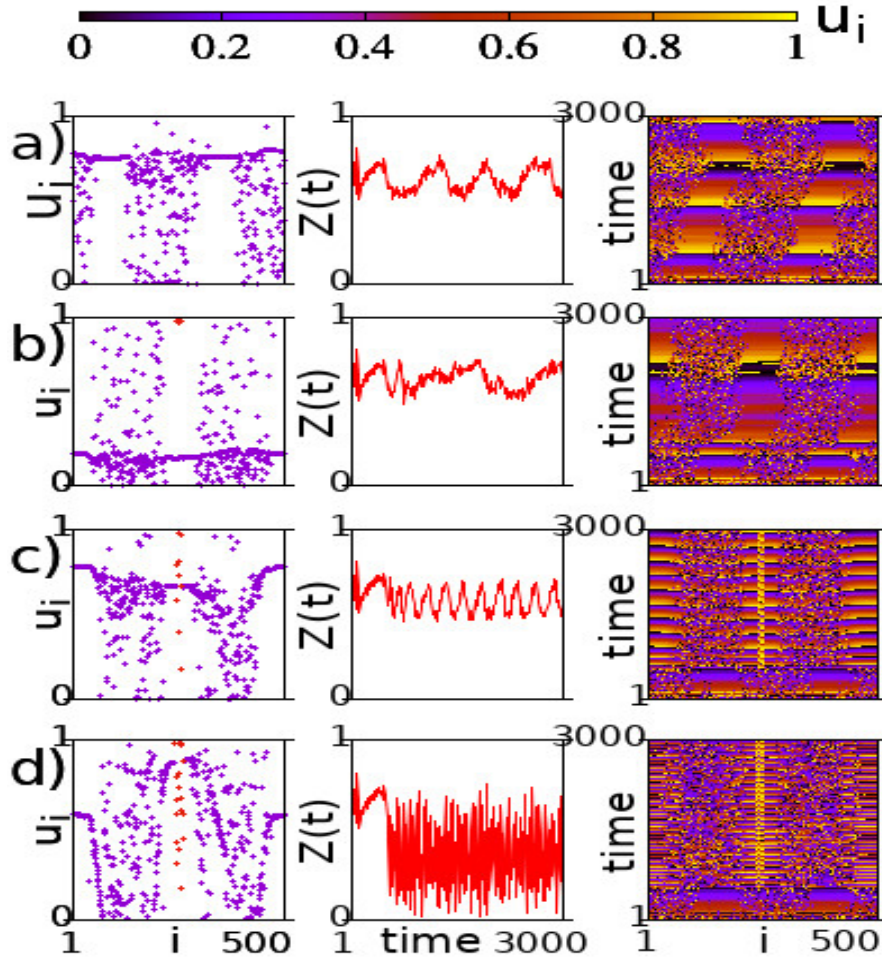


Fig. 3 (Color online) Multichimera state in the LIF network with broken connectivity after 500 TUs: a) $B=0$ (connectivity unbroken for all times), b) $B=1$, c) $B=10$ and d) $B=20$. Typical profile snapshots (left), Kuramoto index (center) and spacetime plots (right panels). The block with broken links is placed symmetrically around the central $i = 250$ oscillator. The coupling constant is $\sigma = 1.7$ and all other parameters are as in Fig. 1. All simulations start from the same initial conditions, chosen randomly between 0 and u_{th} .

thus has the opportunity to create the 2-chimera with one incoherent region centered around the $i = 250$ element, with the two coherent regions to its left and right, while the 2nd incoherent region is located at the left and right corners of the system. At $t = 500$ TUs, the block I_B is introduced. For minimal block size, $B = 1$, Fig. 3b shows that the 2-chimera drifts slowly until one of the coherent regions stabilizes around the block I_B . The position of the

minimal block is not visible in the spacetime plot, but can be spotted as a red point in the potential profile (at the top of the left panel). For block size $B = 10$, Fig. 3c shows a faster drift toward the stable state, where one of the coherent regions surrounds the block. The block is now visible after 500 TUs in the spacetime plot and in the profile (with red dots). Similar conclusions are drawn for Fig. 3d with block size $B = 20$. The evolution of the Kuramoto index follows the same pattern in all four rows up to time $t = 500$ TUs and stabilizes shortly after. The $Z(t)$ index presents more extensive fluctuations for $B = 20$, where the large size of the block with broken connectivity influences the overall synchronization in the system. Comparing the cases for different B values, we find that the Kuramoto index is influenced by the block size B , as also demonstrated in Fig. 4.

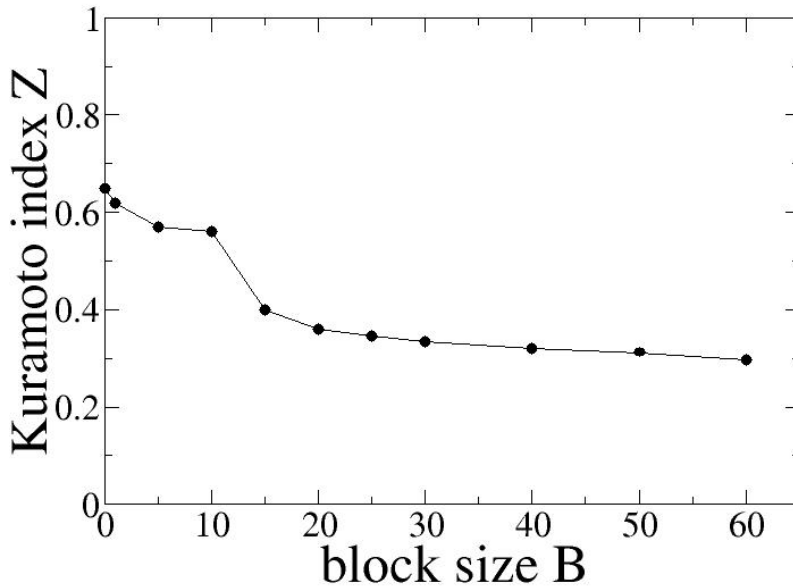


Fig. 4 (Color online) The Kuramoto synchronization index Z as a function of the block size B . The coupling constant is $\sigma = 1.7$ and all other parameters are as in Fig. 1. All realizations start from the same initial conditions, chosen randomly between 0 and u_{th} for each oscillator.

Figure 4 shows that the synchronization index Z decreases as the block size B increases. This can be intuitively expected since the block I_B introduces disorder in the connectivity and thus synchronization decreases in the system. The Z index decreases asymptotically to 0, because even small local common phases may contribute positively to Z , when the system size is finite.

4 The effects of frequency disorder

In this section the nonlocal connectivity is not disturbed but disorder is introduced in the dynamics of the nodes. Namely, the connectivity remains purely nonlocal and the disorder in the frequency of a block of oscillators comes by modifying the threshold potential u_{th} , as explained in Sec. 2.2 and Eq. 5.

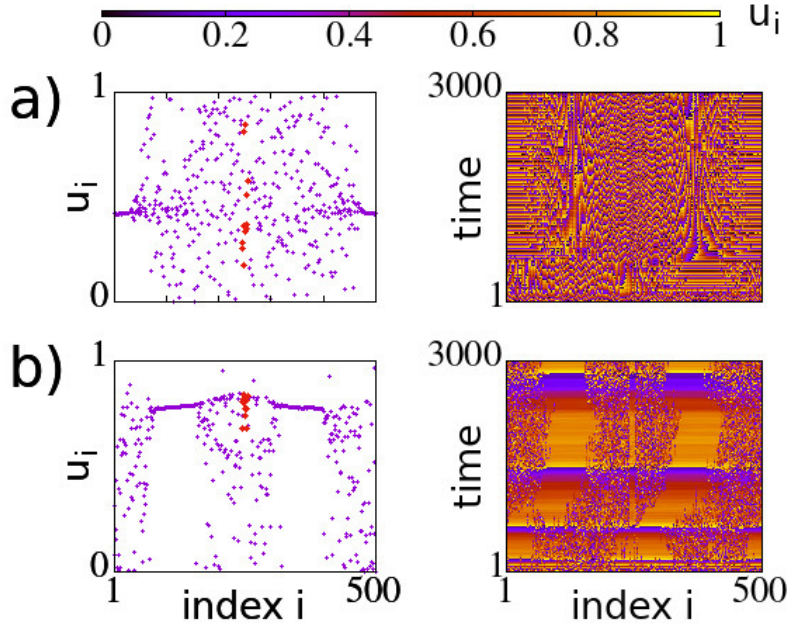


Fig. 5 (Color online) Chimera states in the LIF network with frequency disorder after 500 TUs: a) single chimera for $\sigma = 0.7$ and b) 2-chimera for $\sigma = -1.7$. Typical profile snapshots (left panels) and spacetime plots (right panels). The oscillators in one of the incoherent domains are placed symmetrically around the central $i = 250$ node and are colored red in the profiles (left panels). The threshold potentials are $v_1 = 0.9$ and $v_2 = 0.98$ and the block size is $H = 10$. All other parameters are as in Fig. 1. All simulations start from the same initial conditions, chosen randomly between 0 and $u_{\text{th}}(i)$ for each oscillator.

To investigate the influence of the frequency disorder, we use two threshold values, $v_1 = 0.9$ for the elements that belong to block I_{th} and $v_2 = 0.98$ for all other elements, as in the previous section. To compare the two cases, we use Eq. 2 to calculate the respective periods. For these threshold values, the uncoupled periods are: $T_1 = 2.3$ for the elements in block I_{th} and $T_2 = 3.9$ for the rest of the elements. Alternatively, the block oscillators are 1.7 times faster than the rest.

In Fig. 5, the system starts with unperturbed frequencies and develops a steady state with one coherent and one incoherent domain as in Fig. 1a. After 500 TUs, the frequency disorder is applied and the system is allowed to run

for 2500 additional time steps. The disordered block has size $H = 10$ and all other parameters are as in Fig. 1. As we can see in Fig. 5a, the single chimera pattern shifts so that the incoherent domain is placed symmetrically around the perturbed block I_{th} . This holds true also for the case of the 2-chimera state, which is realized when $\sigma = 1.7$ and is shown in Fig. 5b. Again, the chimera pattern shifts so that the I_{th} block is positioned at the center of one of the two incoherent regions.

To understand the influence of the block size H , we present in Fig. 6 the potential profiles, Kuramoto index and spatiotemporal patterns for different values of H for the single chimera. As in Fig. 5, in all simulations the system starts unperturbed for 500 TUs, after which the I_{th} block is introduced in the system. Even for blocks of minimal disorder, $H = 1$, the spacetime plot in Fig. 6a shows that the pattern shifts slowly until the incoherent part covers symmetrically block I_{th} . The speed of displacement increases as the size of the block increases to $H = 5$ (Fig. 6b) and to $H = 20$ (Fig. 6c). The oscillators in blocks I_{th} are colored red in the profiles and they can be seen in the middle of the incoherent regions. In this case, the Kuramoto synchronization index Z does not significantly change with the block size. Similar conclusions apply to the case of multichimera states (not shown).

It is interesting to note here that while the disorder in the network connectivity drives the coherent regions around the perturbed block, the disorder of the oscillator frequency drives the incoherent regions around the perturbed block. This finding is important for appropriately choosing the correct mechanism when we wish to control the position of a chimera state.

5 Conclusions and Open Problems

Motivated by the diversity of neuronal features and by the different connectivity patterns in biological neuron networks, we investigated here the modifications that the chimera-state patterns undergo under diversification of the threshold potentials or under local modifications in the network connectivity. Using the leaky integrate-and-fire model with nonlocal connectivity, we show that, when the connectivity is destroyed locally in a block of elements, the chimera state pattern shifts until the coherent part of the chimera reaches and surrounds the disordered block. In the case of a multichimera state, again the pattern shifts until one of the coherent domains surrounds the disordered block. For intact nonlocal connectivity, if we modify the threshold potential (or similarly, the period) in a block of elements, the chimera pattern shifts until the incoherent block surrounds the modified block. These results provide us with first evidence about the type of changes that the synchronization patterns undergo, when there are local modifications in the dynamical properties of the neurons or perturbations in the structure of the networks.

The ideas presented here have potential applications in the dynamics of the healthy brain, given that not all neurons are identical, as they are differentiated according to their functional role. The approach in Sec. 4, where a block of

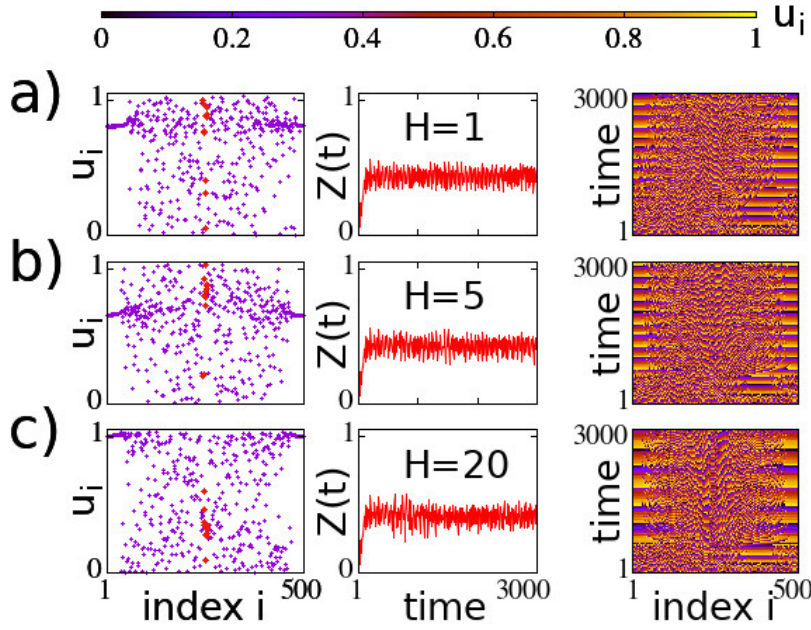


Fig. 6 (Color online) Chimera states in a LIF network with frequency disorder after 500 TUs: a) $H=1$ (minimal disorder), b) $H=5$ and c) $H=20$. Typical profile snapshots (left), Kuramoto synchronization index (center) and spacetime plots (right panels). The oscillators with different frequency are placed symmetrically around the central $i = 250$ node and are colored red in the respective profiles (left panels). The threshold potentials are $v_1 = 0.9$ and $v_2 = 0.98$ and the coupling strength is $\sigma = 0.7$. All other parameters are as in Fig. 1. All simulations start from the same initial conditions, chosen randomly between 0 and $u_{th}(i)$ for each oscillator.

neurons has a different potential threshold than the rest, points to the direction of diversity in the dynamics of the individual neurons. Using more realistic distributions of neuronal thresholds and connectivity schemes resulting from medical imaging experiments, is bound to probe further into the complexity of synchronization patterns in the brain. These complex patterns maybe linked with different functionality modes of the healthy brain.

Open problems include the use of destructed connectivity obtained from medical images of local lesions in the brain. In relation to neuron degenerative disorders, more global deformations in the neuron network connectivity need to be addressed. Diseases such as Alzheimer, Parkinson and Schizophrenia can cause global degeneration in the brain network structure. Medical imaging techniques can be used in all these cases to extract connectivity matrices that reflect the structural (local or global) deformations. When these matrices are used during the dynamical integration, the corresponding synchronization patterns reflect the underlying structural anomalies. Comparison of synchronization patterns between healthy brains and brains suffering from lesions or

from neurodegenerative disorders may offer new tools in the diagnosis of these diseases and/or on their origin and evolution.

Acknowledgements The authors would like to thank Dr. J. Hizanidis, N. D. Tsigkri-DeSmedt and T. Kasimatis for fruitful discussions. A.P. and Ch.G.A. acknowledge support provided by the London Mathematical Society (LMS) Research in Pairs - Scheme 4, Grant No 41903. We acknowledge partial support of this work by the project MIS 5002567, implemented under the “Action for the Strategic Development on the Research and Technological Sector”, funded by the Operational Programme “Competitiveness, Entrepreneurship and Innovation” (NSRF 2014-2020) and co-financed by Greece and the European Union (European Regional Development Fund). This work was supported by computational time granted by the Greek Research & Technology Network (GRNET) at the National HPC Facility - ARIS - under projects Cobrain4 (ID: PR007011) and CoBrain5 (ID: PR009012).

References

1. Y. Kuramoto and D. Battogtokh, Coexistence of coherence and incoherence in nonlocally coupled phase oscillators, *Nonlinear Phenomena in Complex Systems*, **5**, 380 (2002).
2. I. Omelchenko, O. E. Omel'chenko, P. Hövel and E. Schöll, When nonlocal coupling between oscillators becomes stronger: patched synchrony or multichimera states, *Physical Review Letters*, **110**, 224101 (2013).
3. I. Omelchenko, A. Provata, J. Hizanidis, E. Schöll and P. Hövel, Robustness of chimera states for coupled FitzHugh-Nagumo oscillators, *Physical Review E*, **91**, 022917 (2015).
4. Z.-M. Wu, H.-Y. Cheng, Y. Feng, H.-H. Li, Q.-L. Dai and J.-Z. Yang, Chimera states in bipartite networks of FitzHugh–Nagumo oscillators, *Frontiers of Physics*, **13**, 130503 (2018).
5. J. Hizanidis, V. Kanas, A. Bezerianos and T. Bountis, Chimera states in networks of nonlocally coupled Hindmarsh-Rose neuron models, *International Journal of Bifurcation and Chaos*, **24**, 03 (2014).
6. J. Hizanidis, N. E. Kouvaris, G. Zamora-López, A. Díaz-Guilera and C. G. Antonopoulos, Chimera-like States in modular neural networks, *Scientific Reports*, **6**, 19845 (2016).
7. S. Ulonska and I. Omelchenko and A. Zakharova and E. Schöll, Chimera states in networks of Van der Pol oscillators with hierarchical connectivities, *Chaos*, **26**, 094825 (2016).
8. S. Olmi, A. Politi and A. Torcini, Collective chaos in pulse-coupled neural networks, *Europhysics Letters*, **92**, 60007 (2010).
9. S. Lucioli and A. Politi, Irregular collective behavior of heterogeneous neural networks, *Physical Review E*, **105**, 158104 (2010).
10. N. D. Tsigkri-DeSmedt, J. Hizanidis, P. Hövel and A. Provata, Multi-chimera states in the Leaky Integrate-and-Fire model, *Procedia Computer Science*, **66**, 13 (2015).
11. N. D. Tsigkri-DeSmedt, P. Vlamos and A. Provata, Finite size effects in networks of coupled neurons, *Advances in Experimental Medicine and Biology*, **1194**, 397–407 (2020).
12. A. Schmidt, T. Kasimatis, J. Hizanidis, A. Provata, and P. Hövel, Chimera patterns in two-dimensional networks of coupled neurons, *Physical Review E*, **95**, 032224 (2017).
13. T. Kasimatis, J. Hizanidis and A. Provata, Three-dimensional chimera patterns in networks of spiking neuron oscillators, *Physical Review E*, **97**, 052213 (2018).
14. Y. Maistrenko, O. Sudakov, O. Osiv, and V. Maistrenko, Chimera states in three dimensions, *New Journal of Physics*, **17**, 073037 (2015).
15. V. Maistrenko, O. Sudakov, O. Osiv, Y. Maistrenko, Multiple scroll wave chimera states, *European Physical Journal: Special Topics*, **226**, 1867-1881 (2017).
16. N. D. Tsigkri-DeSmedt, J. Hizanidis, P. Hövel and A. Provata, Multi-Chimera States and Transitions in the Leaky Integrate-and-Fire Model with Nonlocal Coupling and Hierarchical Connectivity, *European Physical Journal Special Topics*, **225**, 1149–1164 (2016).
17. G. Argyropoulos and A. Provata, Chimera States With 2D Deterministic and Random Fractal Connectivity, *Frontiers in Applied Mathematics and Statistics*, **5**,35 (2019).

18. R. G. Andrzejak, G. Ruzzene, E. Schöell and I. Omelchenko, Two populations of coupled quadratic maps exhibit a plentitude of symmetric and symmetry broken dynamics, *Chaos*, **30**, 033125 (2020).
19. C. G. Antonopoulos, S. Srivastava, S. E. S. Pinto and M. S. Baptista, Do Brain Networks Evolve by Maximizing Their Information Flow Capacity?, *PLoS Computational Biology*, **11**, e1004372 (2015).
20. E. Sigalas, J. Li, A. Bezerianos and Ch. G. Antonopoulos, Emergence of chimera-like states in prefrontal-cortex macaque intracranial recordings, in Proceedings of the “2018 International Workshop on Pattern Recognition in Neuroimaging (PRNI)”, Singapore, p.p. 1-4 (2018).
21. I. Koulierakis, D. A. Verganelakis, I. Omelchenko, A. Zakharova, E. Schöll and A. Provata, Structural anomalies in brain networks induce dynamical pacemaker effects, *accepted to Chaos* (2020).
22. M. J. Panaggio and D. Abrams, Chimera states: coexistence of coherence and incoherence in networks of coupled oscillators, *Nonlinearity*, **28**, R67 (2015).
23. E. Schöll, Synchronization patterns and chimera states in complex networks: interplay of topology and dynamics, *European Physical Journal Special Topics*, **225**, 891–919 (2016).
24. O. E. Omel’Chenko, The mathematics behind chimera states, *Nonlinearity*, **31**, R121 (2018).
25. P. Katsaloulis, D. A. Verganelakis, A. Provata, Fractal dimension and lacunarity of tractography images of the human brain, *Fractals* **17** 181-189 (2009).
26. P. Expert, R. Lambiotte, D. Chialvo, K. Christensen, H. J. Jensen, D. J. Sharp, F. Turkheimer, Self-similar correlation function in brain resting-state functional magnetic resonance imaging, *Journal of the Royal Society Interface*, **8** 472-479 (2011).
27. P. Katsaloulis, A. Ghosh, A. C. Philippe, A. Provata, R. Deriche, Fractality in the neuron axonal topography of the human brain based on 3-D diffusion MRI, *European Physical Journal B* **85**, 150 (2012).
28. A. Plerou and P. Vlamos, Evaluation of mathematical cognitive functions with the use of EEG brain imaging, *Experimental Multimedia Systems for Interactivity and Strategic Innovation*, 284-306 (2015).
29. M. Psiha and P. Vlamos, Modeling neural circuits in Parkinson’s disease, *Advances in Experimental Medicine and Biology*, **822** 139–147 (2015).
30. A. Plerou, P. Vlamos, and A. Margetaki, EEG analysis of the neurofeedback training effect in algorithmic thinking, *Advances in Experimental Medicine and Biology* **988** 313–324 (2017).
31. F. Mormann, K. Lehnertz, P. David, and C. E. Elger, Mean phase coherence as a measure for phase synchronization and its application to the EEG of epilepsy patients, *Physica D* **144**, 358 (2000).
32. F. Mormann, T. Kreuz, R. G. Andrzejak, P. David, K. Lehnertz, and C. E. Elger, Epileptic seizures are preceded by a decrease in synchronization, *Epilepsy Research* **53**, 173–185 (2003).
33. R. G. Andrzejak, C. Rummel, F. Mormann and K. Schindler, All together now: Analogies between chimera state collapses and epileptic seizures, *Scientific Reports*, **6**, 23000 (2016).
34. N. C. Rattenborg, C. J. Amlaner and S. L. Lima, Behavioral, neurophysiological and evolutionary perspectives on unihemispheric sleep, *Neuroscience and Biobehavioral Reviews*, **24**, 817 (2000).
35. N. C. Rattenborg, D. Martinez-Gonzalez, J. A. Lesku and M. Scriba, A bird’s eye view of sleep, *Science*, **322**, 527, (2008).
36. T. Isele, J. Hizanidis, A. Provata and P. Hövel, Controlling chimera states: The influence of excitable units, *Physical Review E*, **93**, 022217 (2016).
37. G. Ruzzene, I. Omelchenko, E. Schöll, A. Zakharova and R. G. Andrzejak, Controlling chimera states via minimal coupling modification, *Chaos*, **29**, 0511031 (2019).
38. N. Brunel and M. C. W. van Rossum, Lapicque’s 1907 paper: from frogs to integrate-and-fire *Brain Research Bulletin*, **50**, 303–304 (1999).
39. L. F. Abbott, Lapicque’s introduction of the integrate-and-fire model neuron (1907) *Biological Cybernetics*, **97**, 337 (2007).
40. F. P. Kemeth, S. W. Haugland, L. Schmidt, I. G. Kevrekidis and K. Krischer, A classification scheme for chimera states, *Chaos*, **26**, 094815(2016).

-
41. N. D. Tsigkri-DeSmedt, J. Hizanidis, E. Schöll, P. Hövel and A. Provata, Chimera states in the Leaky Integrate-and-Fire Model: Effects of Reflecting Connectivity, *European Physical Journal B*, **90:139**, (2017).
 42. N. D. Tsigkri-DeSmedt, I. Koulierakis, G. Karakos and A. Provata, Synchronization patterns in LIF neuron networks: merging nonlocal and diagonal connectivity, *European Physical Journal B*, **91**, 305 (2018).